DQ-Frame Modeling of an Active Power Filter Integrated With a Grid-Connected, Multifunctional Electric Vehicle Charging Station

Russell Crosier, *Student Member, IEEE*, and Shuo Wang, *Senior Member, IEEE*

***Abstract*—The paper first proves the existence of a nonlinear, feedback loop due to the effect of an active power filter (APF) on the grid voltage for a multifunctional electric vehicle charging station. A linear, open-loop model is derived based on direct quadrature (DQ)-theory in discrete time (DT). Based on this model, a linear, closed-loop model is further developed with DQ-theory in DT. A triangle-hold equivalent instead of a zero-order-hold equivalent is employed in the model for better representation. The developed linear, closed-loop model is finally generalized to general power systems. Simulations are carried out to verify the developed models under transient conditions. The short-time (1–2 ms), transient stability of the grid with an APF is determined with the developed model. In contrast to existing stability analyses in the phasor domain, using DQ-theory can linearize the loop and simplify the loop model in DT domain.**

***Index Terms*—Active power filter, direct-quadrature (DQ)-frame, electric vehicle (EV) charging, power system stability, triangle-hold equivalent.**

I. Introduction

With the expected growth of high-tech loads and the increasing scrutiny given to voltage quality, active power filters (APFs) are expected to play an increasingly important role in power distribution and delivery [11]. This fact and the availability of new power electronics technologies have led the field of APFs to become very diverse in terms of system size and configuration [1], [2], [12]. Also, the desire for large pieces of infrastructure to serve more than one purpose implies that APF functionality will be found in grid interfaces built for a different primary purpose. For example, a multifunctional electric vehicle (EV) charging station of multimegawatt capacity is presented in [12], [16], and [17], and because of its high power level, it was decided that it should be connected directly to medium voltage (MV) levels and that it should also provide harmonic and reactive power compensation of the grid current.

By removing reactive and harmonic currents from the grid, APFs improve voltage quality and lower the RMS loading which decreases I^2R losses and increases effective capacity and steady-state stability margins. However, with the increasing proliferation of power electronic-based grid interfaces, localized, transient stability due to their interaction with the grid is becoming a general concern.

The EV charging station/APF mentioned earlier is a prime example of a large APF that could result in grid voltage instability. Because of its multimegawatt size, it cannot be considered to be connected to an infinite bus. On the contrary, its output current will have a significant effect on system voltage (after all reactive and harmonic compensation is *supposed* to improve voltage quality). Because the grid voltage is part of the control input for an APF, this introduces a parasitic feedback loop. For certain classes of APF [12]–[14], this feedback loop is nonlinear and, thus far, has not been fully analyzed.

Closed-loop, transient instability has been recognized as a concern for large, grid-connected, equipment [3]. In addition, some points on the grid are highly susceptible to instability due to local resonance [22]. In the past, large APFs, such as [12], had negligible presence on the grid. Since the publication of [3], the problem of closed-loop stability has been analyzed for flexible ac transmission systems (FACTS) such as static synchronous compensators (STATCOMs) and static VAR compensators (SVCs) [4]. However, despite the growing size and prevalence of APFs, the issue of closed-loop stability has not yet been addressed for them in general.

For certain classes of APFs [5], [6], [15], [21] the problem of stability is much easier to solve. This is because these APFs have output current that is linear, time-invariant (LTI)-related to the other currents and voltages, i.e., they behave like linear elements, allowing a low impedance path for load harmonics. Therefore, these APFs can be integrated into the grid model as just another linear element of the network. However, the functionality of these APFs is limited because they cannot identify reactive or negative-sequence currents (which are nonlinear functions of the grid voltage), which [12] can do. Therefore, it is desirable that the APFs use the grid voltage to identify its reference current. Despite the superior capabilities of APFs in this class, a dynamic model for the closed-loop interaction of these APFs with a grid impedance has not been published.

With the exception of [19], which is the conference paper on which this paper is based, the publication most closely related to this closed-loop issue is [20]. In this paper, the authors consider the closed-loop interaction of an active, pulse width modulation (PWM)-based rectifier (with dynamic power control based on DQ-theory) with a weak grid. However, the rectifier only draws active power, and the additional complexity introduced by APF functionality is not considered. Additionally, the grid interaction

Manuscript received October 24, 2012; revised December 22, 2012; accepted January 19, 2013. Date of current version June 6, 2013. This work was supported by the National Science Foundation under the award number ECCS-1151126. Recommended for publication by Associate Editor O. C. Onar.

The authors are with the Department of Electrical and Computer Engineering, University of Texas-San Antonio, San Antonio, TX 78249 USA (e-mail: mtb892@my.utsa.edu; shuowang@ieee.org).

Digital Object Identifier 10.1109/TPEL.2013.2245515

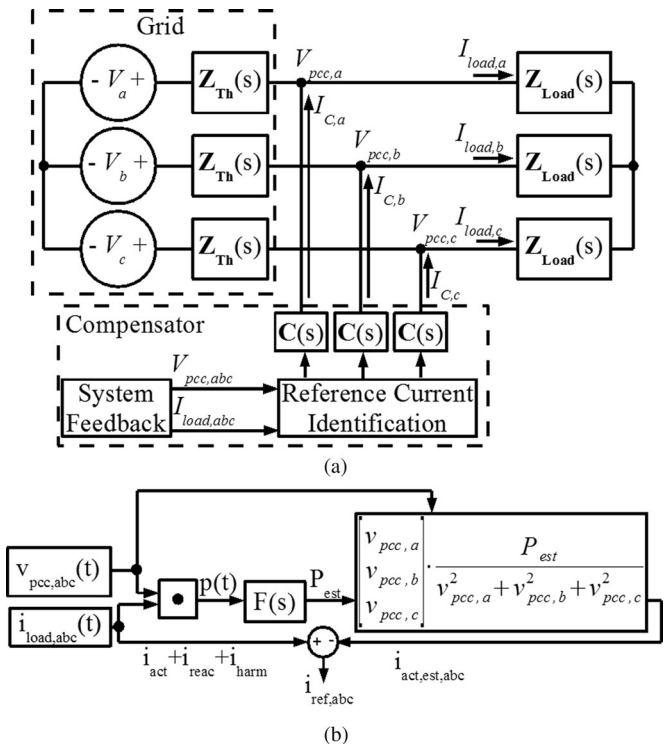

Fig. 1. Multifunctional EV charging station in grid compensation mode. (a) Closed-loop system model and (b) reference current identification algorithm.

is only considered for a specific, very simple grid model. Finally, a nonlinear analysis is used, which is in contrast to the analysis herein which transforms the closed loop into an LTI problem.

In this paper and in the conference paper [19] on which this paper is based, the nonlinear, closed-loop issue is explained. Then, a procedure is derived to integrate the APF in [12], [16], and [17] into a simple power system and transform the closed-loop model to a linear framework. This procedure is then generalized. The equations resulting from this generalization can be applied to any power system and any discrete time (DT)-controlled APF that can be modeled in the DQ-frame. However, this paper has the following additions and improvements: 1), Sections III-D and IV-B were added in order to model in state-space a load being connected to the system at any time instead of a state-space model based on a load that has always been connected; 2), Section V has been completely redone to simulate a system with "transient" load in order to verify the math in the new Sections III-D and IV-B; 3), Section III-E has been added to justify certain assumptions that are taken for granted in [19]; 4), Section V-B has been added to Section V to further justify those assumptions with simulation; 5), Section VI has been added in order to explain the difficulty in attaining experimental results for this application at this stage and to propose a verification experiment; and finally 6), minor changes been made to increase clarity.

II. Nonlinear, Closed Loop

Fig. 1(a) shows an example of a multifunctional EV charging station [12], [16], which is tied to a MV power grid, under APF mode. It will be shown in this section that it results in a nonlinear system model. The derivation of this model starts with deriving the APF's output current, I_C, as a function of $V_{\rm pcc}$ and $I_{\rm load}$, (1)–(9), and (11). In (11) $C(s)$, the transfer function between the reference and output currents of the APF, is introduced. In (10), $V_{\rm pcc}$ is written as a function of I_C. Then, (10) and (11) are combined to form the closed-loop model of $V_{\rm pcc}$. The closed-loop model is written in its final form in (13).

As shown in Fig. 1(b), the point of common coupling (PCC) voltage is used to identify the active current. First, the instantaneous power is determined by the dot-product of the three-phase PCC voltage and load current

$$p(t) = \begin{bmatrix} v_{\rm pcc,a} & v_{\rm pcc,b} & v_{\rm pcc,c} \end{bmatrix} \begin{bmatrix} i_{\rm load,a} \\ i_{\rm load,b} \\ i_{\rm load,c} \end{bmatrix} \tag{1}$$

where $p(t)$ is the instantaneous power of the load.

Then, the active power is estimated by passing the determined instantaneous power through a low-pass filter, $F(s)$

$$P_{\rm est}(s) = L\{p(t)\} \cdot F(s) \tag{2}$$

where $P_{\rm est}(s)$ is the estimated power in the Laplace domain and $L\{\}$ is the Laplace transform of the instantaneous power from (1). We can also write (2) in the time-domain as

$$p_{\rm est}(t) = \int_0^\infty p(t-\tau) \cdot f(\tau) d\tau \tag{3}$$

where $f(t)$ is the time-domain impulse response of the filter $F(s)$. Having estimated the active power, the active current estimate can be written as [12]

$$\begin{bmatrix} i_{\rm act,est,a} \\ i_{\rm act,est,b} \\ i_{\rm act,est,c} \end{bmatrix} = \begin{bmatrix} v_{\rm pcc,a} \\ v_{\rm pcc,b} \\ v_{\rm pcc,c} \end{bmatrix} \frac{p_{\rm est}(t)}{v_{\rm pcc,a}^2 + v_{\rm pcc,b}^2 + v_{\rm pcc,c}^2}$$

or more compactly as

$$i_{\rm act,est,abc} = v_{\rm pcc,abc} \frac{p_{\rm est}(t)}{v_{\rm pcc,abc}^T \cdot v_{\rm pcc,abc}} \tag{4}$$

where $i_{\rm act,est,abc} = \begin{bmatrix} i_{\rm act,est,a} \\ i_{\rm act,est,b} \\ i_{\rm act,est,c} \end{bmatrix}$ and $v_{\rm pcc,abc} = \begin{bmatrix} v_{\rm pcc,a} \\ v_{\rm pcc,b} \\ v_{\rm pcc,c} \end{bmatrix}$.

Finally, (1), (3), and (4) can be combined to yield

$$i_{\rm act,est,abc} = v_{\rm pcc,abc} \times \frac{\int_0^\infty v_{\rm pcc,abc}^T(t-\tau) \cdot i_{\rm load,abc}(t-\tau) \cdot f(\tau) d\tau}{v_{\rm pcc,abc}^T \cdot v_{\rm pcc,abc}}. \tag{5}$$

Ideally, the compensator should supply all of the undesired components of the load current $i_{\rm undes}$ in Fig. 1(b), but none of the load's active current $i_{\rm act}$. Therefore, the reference current for the compensator is defined as

$$i_{{\rm ref},abc} = i_{{\rm load},abc} - i_{{\rm act,est},abc}. \tag{6}$$

Combining (5) and (6) yields the final expression for the reference current

$$i_{{\rm ref},abc} = i_{{\rm load},abc} - v_{\rm pcc,abc} \times \frac{\int_0^\infty v_{\rm pcc,abc}^T(t-\tau) \cdot i_{\rm load,abc}(t-\tau) \cdot f(\tau) d\tau}{v_{\rm pcc,abc}^T \cdot v_{\rm pcc,abc}}. \tag{7}$$

Definition (6) makes sense if the load current is separated into active and undesired components [as in Fig. 1(b)]. Doing this to (6) yields

$$i_{\mathrm{ref},abc} = i_{\mathrm{act},abc} + i_{\mathrm{undes},abc} - i_{\mathrm{act,est},abc}. \tag{8}$$

Since $i_{\mathrm{act},abc} - i_{\mathrm{act,est},abc} \approx 0$, (8) can be approximated as

$$i_{\mathrm{ref},abc} \approx i_{\mathrm{undes},abc}. \tag{9}$$

Therefore, definition (6) serves to leave only the undesired components of the load current (the components that the grid should not supply) in the reference current of the compensator. The goal of estimating the active current was so that it could be removed as accurately as possible from (8). The reference current should only contain $i_{\mathrm{undes},abc}$ because the goal of compensation is to remove everything but the active current from the grid.

To incorporate the APF into the power system, the PCC voltage is written as a function of the grid voltage $V_{g,abc}$ and the compensator output current based on Fig. 1(a)

$$V_{\mathrm{pcc},abc}(s) = V_{g,abc}(s)\frac{Z_{\mathrm{Load}}(s)}{Z_{\mathrm{Load}}(s)+Z_{\mathrm{Th}}(s)} + I_{C,abc}(s)\frac{Z_{\mathrm{Load}}(s)\cdot Z_{\mathrm{Th}}(s)}{Z_{\mathrm{Load}}(s)+Z_{\mathrm{Th}}(s)}$$

where $Z_{\mathrm{Th}}(s)$ is the Thevenin impedance of the grid and $Z_{\mathrm{Load}}(s)$ is the impedance of the load. This can be simplified as

$$V_{\mathrm{pcc},abc}(s) = \frac{Z_{\mathrm{Load}}(s)}{Z_{\mathrm{Load}}(s)+Z_{\mathrm{Th}}(s)} \times \left(V_{g,abc}(s) + I_{C,abc}(s)\cdot Z_{\mathrm{Th}}(s)\right). \tag{10}$$

To close the loop, $I_{C,abc}(s)$ needs to be written in terms of the other system variables

$$I_{C,abc}(s) = C(s)\cdot I_{\mathrm{ref},abc}(s) = C(s)\cdot L\left\{ i_{\mathrm{load},abc} - v_{\mathrm{pcc},abc}\frac{\int_0^\infty v^T_{\mathrm{pcc},abc}(t-\tau)\cdot i_{\mathrm{load},abc}(t-\tau)\cdot f(\tau)d\tau}{v^T_{\mathrm{pcc},abc}\cdot v_{\mathrm{pcc},abc}}\right\} \tag{11}$$

where $L\{\}$ is the Laplace transform operator and $C(s)$ is the dynamics of the compensator. Now the loop can be closed by combining (10) and (11)

$$V_{\mathrm{pcc},abc}(s) = \frac{Z_{\mathrm{Load}}(s)}{Z_{\mathrm{Load}}(s)+Z_{\mathrm{Th}}(s)}\left(V_{g,abc}(s) + C(s)\cdot L\left\{ i_{\mathrm{load},abc} - v_{\mathrm{pcc},abc} \times \frac{\int_0^\infty v^T_{\mathrm{pcc},abc}(t-\tau)\cdot i_{\mathrm{load},abc}(t-\tau)\cdot f(\tau)d\tau}{v^T_{\mathrm{pcc},abc}\cdot v_{\mathrm{pcc},abc}}\right)\cdot Z_{\mathrm{Th}}(s)\right\}. \tag{12}$$

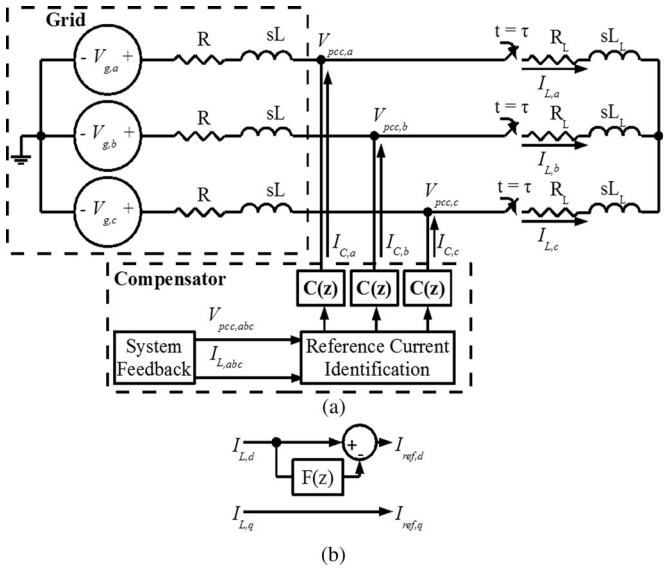

Fig. 2. Simple power system incorporating the APF of a multifunctional EV charging station. (a) Function diagram and (b) DQ-frame equivalent of the reference current.

The final step is to write $i_{\mathrm{load},abc}$ in terms of $v_{\mathrm{pcc},abc}$. Letting $Y_{\mathrm{Load}}(s)$ be the reciprocal of $Z_{\mathrm{Load}}(s)$ in Fig. 1(a), it can be seen that $I_{\mathrm{load}}(s) = V_{\mathrm{pcc}}(s)\cdot Y_{\mathrm{Load}}(s)$ for each phase. This yields the following expression for all three phases in the time domain:

$$i_{\mathrm{load},abc}(t) = \int_0^\infty v_{\mathrm{pcc},abc}(t-u)\cdot y_{\mathrm{Load}}(u)du.$$

Substituting this expression into (12) yields (13) as shown at the bottom of the next page.

Looking inside the L operator in (13), it can be seen that nonlinear operations occur on $v_{\mathrm{pcc},abc}$ and $i_{\mathrm{load},abc}$. This is due to multiplications in (1) and (4). Because these nonlinear operations occur on variables, the L operator will not yield a purely algebraic expression. Therefore, the system model is nonlinear, and its stability cannot be analyzed by transfer function methods alone.

III. Deriving a Linear, Closed Loop

A. Open-Loop System Model

Fig. 2 shows a DT (Z-domain)-controlled APF integrated into a simple, balanced power system. Before the load is applied ($t < \tau$), the PCC voltage is equal to the grid voltage, $v_{g,abc}$ because the line current, i_{abc}, is zero. Letting $V_G(s)$ denote the grid voltage, $V_{\mathrm{pcc}}(s)$ the PCC voltage, $I_L(s)$ the load current, $I_G(s)$ the grid current, and $I_C(s)$ the compensation current injected to the grid from the APF; the following transfer functions are written to model the open-loop system after the switch is closed

$(t \geq \tau)$:

$$\begin{cases} \dfrac{V_{\rm pcc}(s)}{V_G(s)} = \dfrac{R_L + sL_L}{s\,(L+L_L)+(R+R_L)} \\ \dfrac{V_{\rm pcc}(s)}{I_C(s)} = \dfrac{(R+sL)\,(R_L+sL_L)}{s\,(L+L_L)+(R+R_L)} \\ \dfrac{I_L(s)}{V_G(s)} = \dfrac{1}{s\,(L+L_L)+(R+R_L)} \\ \dfrac{I_L(s)}{I_C(s)} = \dfrac{R+sL}{s\,(L+L_L)+(R+R_L)}. \end{cases} \tag{14}$$

Therefore, using superposition,

$$\begin{aligned} V_{\rm pcc}(s) &= \frac{R_L+sL_L}{s\,(L+L_L)+(R+R_L)}V_G(s) \\ &\quad + \frac{(R+sL)\,(R_L+sL_L)}{s\,(L+L_L)+(R+R_L)}I_C(s) \\ I_L(s) &= \frac{1}{s\,(L+L_L)+(R+R_L)}V_G(s) \\ &\quad + \frac{R+sL}{s\,(L+L_L)+(R+R_L)}I_C(s). \end{aligned} \tag{15}$$

Then according to the procedure given in [10, Sec. 4.4], this can be written in the time domain as

$$\begin{aligned} \frac{d}{dt}\begin{bmatrix} x_1 \\ x_2 \end{bmatrix} &= \begin{bmatrix} a_1 & 0 \\ 0 & a_1 \end{bmatrix}\begin{bmatrix} x_1 \\ x_2 \end{bmatrix} + \begin{bmatrix} a_2 & a_3 \\ a_4 & 1 \end{bmatrix}\begin{bmatrix} i_C \\ v_g \end{bmatrix} \\ \begin{bmatrix} v_{\rm pcc} \\ i_L \end{bmatrix} &= \begin{bmatrix} a_5 & 0 \\ 0 & a_5 \end{bmatrix}\begin{bmatrix} x_1 \\ x_2 \end{bmatrix} + \begin{bmatrix} a_6 & a_7 \\ a_8 & 0 \end{bmatrix}\begin{bmatrix} i_C \\ v_g \end{bmatrix} \\ &\quad + \begin{bmatrix} a_9 \\ 0 \end{bmatrix}\frac{d}{dt}(i_C). \end{aligned} \tag{16}$$

where

$$\begin{aligned} a_1 &= \frac{-R-R_L}{L+L_L}, \quad a_2 = -\frac{(R_LL - RL_L)^2}{(L+L_L)^2} \\ a_3 &= \frac{R_LL - RL_L}{L+L_L}, \quad a_4 = -a_3 \\ a_5 &= \frac{1}{L+L_L}, \quad a_6 = \frac{RL_L^2 + R_LL^2}{(L+L_L)^2}, \quad a_7 = \frac{L_L}{L+L_L} \\ a_8 &= \frac{L}{L+L_L}, \quad a_9 = \frac{LL_L}{L+L_L} \end{aligned}$$

and x_1 and x_2 are internal variables of the system.

In (16), the primary output of interest is $v_{\rm pcc}$, but the output i_L is also included. This is because i_L in the loop of Fig. 2(a) will be closed in Section III-B. Since i_C is a function of i_L in Fig. 2(a), i_L is needed to close this loop. However, when the loop is closed at the end of Section III-B, i_L will no longer appear as an output because it is no longer needed.

Since (16) is a per-phase representation of a balanced system, the equation in the ABC-frame is

$$\begin{aligned} \frac{d}{dt}\begin{bmatrix} x_{1,abc} \\ x_{2,abc} \end{bmatrix} &= \begin{bmatrix} (a_1)_{3\times3} & 0_{3\times3} \\ 0_{3\times3} & (a_1)_{3\times3} \end{bmatrix}\begin{bmatrix} x_{1,abc} \\ x_{2,abc} \end{bmatrix} \\ &\quad + \begin{bmatrix} (a_2)_{3\times3} & (a_3)_{3\times3} \\ (a_4)_{3\times3} & I_{3\times3} \end{bmatrix}\begin{bmatrix} i_{C,abc} \\ v_{g,abc} \end{bmatrix} \\ \begin{bmatrix} v_{{\rm pcc},abc} \\ i_{L,abc} \end{bmatrix} &= \begin{bmatrix} (a_5)_{3\times3} & 0_{3\times3} \\ 0_{3\times3} & (a_5)_{3\times3} \end{bmatrix}\begin{bmatrix} x_{1,abc} \\ x_{2,abc} \end{bmatrix} \\ &\quad + \begin{bmatrix} (a_6)_{3\times3} & (a_7)_{3\times3} \\ (a_8)_{3\times3} & 0_{3\times3} \end{bmatrix}\begin{bmatrix} i_{C,abc} \\ v_{g,abc} \end{bmatrix} \\ &\quad + \begin{bmatrix} (a_9)_{3\times3} \\ 0_{3\times3} \end{bmatrix}\frac{d}{dt}(i_{C,abc}) \end{aligned} \tag{17}$$

where the notation $(u)_{3\times3}$ indicates a diagonal matrix with u on the diagonal.

The next step is to transform the system into the DQ0-frame. According to [9], when the following conventions are used

$$\begin{aligned} &y_{dq0} = T_{dq0}\,y_{abc}, \quad y_{abc} = T_{dq0}^{-1}\,y_{dq0} \\ &T_{dq0} = \frac{2}{3} \\ &\quad \times \begin{bmatrix} \cos(\omega t+\phi) & \cos(\omega t+\phi-120^\circ) & \cos(\omega t+\phi+120^\circ) \\ \sin(\omega t+\phi) & \sin(\omega t+\phi-120^\circ) & \sin(\omega t+\phi+120^\circ) \\ 1/2 & 1/2 & 1/2 \end{bmatrix} \\ &T_{dq0}^{-1} = \begin{bmatrix} \cos(\omega t+\phi) & \sin(\omega t+\phi) & 1 \\ \cos(\omega t+\phi-120^\circ) & \sin(\omega t+\phi-120^\circ) & 1 \\ \cos(\omega t+\phi+120^\circ) & \sin(\omega t+\phi+120^\circ) & 1 \end{bmatrix} \end{aligned} \tag{18}$$

and ϕ is defined such that $v_{g,a} = V_g\cos(\omega t+\varphi)$ (indicating that the DQ-frame is aligned to the grid voltage), then the following is true:

$$\begin{aligned} &\frac{d}{dt}(\alpha_{abc}) = (u)_{3\times3}\,\alpha_{abc} + (v)_{3\times3}\,\beta_{abc} \\ &\qquad\qquad \downarrow \\ &\frac{d}{dt}(\alpha_{dq0}) = \begin{bmatrix} u & -\omega & 0 \\ \omega & u & 0 \\ 0 & 0 & u \end{bmatrix}\alpha_{dq0} + (v)_{3\times3}\begin{bmatrix} \beta_d \\ \beta_q \\ 0 \end{bmatrix} \end{aligned} \tag{19}$$

where the equation before the arrow represents any first-order, balanced, three-phase system, and β_{abc} is a three-phase-

$$V_{{\rm pcc},abc}(s) = \frac{Z_{\rm load}(s)}{Z_{\rm load}(s)+Z_{\rm Th}(s)}\left(V_{g,abc}(s) + C(s)\cdot\left(\frac{v_{{\rm pcc},abc}(s)}{z_{\rm Load}(s)} - L\cdot\left\{v_{{\rm pcc},abc}\right.\right.\right.$$
$$\left.\left.\left. \cdot\,\frac{\int_0^\infty v_{{\rm pcc},abc}^T(t-\tau)\cdot\left[\int_0^\infty v_{{\rm pcc},abc}(t-\tau-u)\cdot y_{\rm Load}(u)\cdot du\right]\cdot f(\tau)d\tau}{v_{{\rm pcc},abc}^T\cdot v_{{\rm pcc},abc}}\right\}\right)\cdot Z_{\rm Th}(s)\right) \tag{13}$$

balanced, driving function. Also, in particular

$$v_{g,dq0} = T_{dq0} v_{g,abc} = \begin{bmatrix} V_g \\ 0 \\ 0 \end{bmatrix}. \tag{20}$$

Because β_0 is zero in (19), the last line of the DQ0-frame expression is essentially $0 = 0$. Therefore, the DQ-frame can be used instead of the DQ0-frame

$$\begin{aligned} \frac{d}{dt}(\alpha_{abc}) &= (u)_{3\times 3}\,\alpha_{abc} + (v)_{3\times 3}\,\beta_{abc} \rightarrow \frac{d}{dt}(\alpha_{dq}) \\ &= \begin{bmatrix} u & -\omega \\ \omega & u \end{bmatrix} \alpha_{dq} + (v)_{2\times 2}\beta_{dq} \end{aligned} \tag{21}$$

where $y_{dq} = T_{dq} y_{abc}$, $z_{dq} = T_{dq} z_{abc}$, and

$$T_{dq} = \frac{2}{3}\begin{bmatrix} \cos(\omega t+\phi) & \cos(\omega t+\phi-120^\circ) & \cos(\omega t+\phi+120^\circ) \\ \sin(\omega t+\phi) & \sin(\omega t+\phi-120^\circ) & \sin(\omega t+\phi+120^\circ) \end{bmatrix}.$$

Therefore, (21) can be applied to (17) to transform (17) into the DQ-frame

$$\begin{aligned} \frac{d}{dt}\begin{bmatrix} x_{1,dq} \\ x_{2,dq} \end{bmatrix} &= A\begin{bmatrix} x_{1,dq} \\ x_{2,dq} \end{bmatrix} + B\begin{bmatrix} i_{C,dq} \\ v_{g,dq} \end{bmatrix} \\ \begin{bmatrix} v_{\mathrm{pcc},dq} \\ i_{L,dq} \end{bmatrix} &= C\begin{bmatrix} x_{1,dq} \\ x_{2,dq} \end{bmatrix} + D\begin{bmatrix} i_{C,dq} \\ v_{g,dq} \end{bmatrix} + F\frac{d}{dt} i_{C,dq} \end{aligned} \tag{22}$$

where

$$A = \begin{bmatrix} \begin{bmatrix} a_1 & -\omega \\ \omega & a_1 \end{bmatrix} & 0_{2\times 2} \\ 0_{2\times 2} & \begin{bmatrix} a_1 & -\omega \\ \omega & a_1 \end{bmatrix} \end{bmatrix}, B = \begin{bmatrix} (a_2)_{2\times 2} & (a_3)_{2\times 2} \\ (a_4)_{2\times 2} & I_{2\times 2} \end{bmatrix}$$

$$C = \begin{bmatrix} (a_5)_{2\times 2} & 0_{2\times 2} \\ 0_{2\times 2} & (a_5)_{2\times 2} \end{bmatrix}, D = \begin{bmatrix} \begin{bmatrix} a_6 & a_9\omega \\ -a_9\omega & a_6 \end{bmatrix} & (a_7)_{2\times 2} \\ (a_8)_{2\times 2} & 0_{2\times 2} \end{bmatrix}$$

$$F = \begin{bmatrix} (a_9)_{2\times 2} \\ 0_{2\times 2} \end{bmatrix}.$$

Also, because

$$v_{dq0}^T i_{dq0} = v_{abc}^T T_{dq0}^T T_{dq0} i_{abc} = v_{abc}^T \frac{2}{3} I_{3x3} i_{abc} = \frac{2}{3} p(t)$$

the three-phase, instantaneous power is given by

$$p(t) = \frac{3}{2}(v_d i_d + v_q i_q + v_0 i_0) = \frac{3}{2} V_d i_d. \tag{23}$$

Equation (23) is true because the DQ-frame is aligned to the grid voltage, and, therefore, v_q and v_0 disappear. Hence, power is proportional to i_d and is not a function of i_q.

For reasons given in Section III-B, the system needs to be modeled in DT. Therefore, the third step is to transform (22) to DT. To do this, the output variables are redefined by removing the term $F\frac{d}{dt} i_{C,dq}$[this term will be restored in (26)]

$$\begin{bmatrix} v'_{\mathrm{pcc},dq} \\ i'_{L,dq} \end{bmatrix} = C\begin{bmatrix} x_{1,dq} \\ x_{2,dq} \end{bmatrix} + D\begin{bmatrix} i_{C,dq} \\ v_{g,dq} \end{bmatrix}. \tag{24}$$

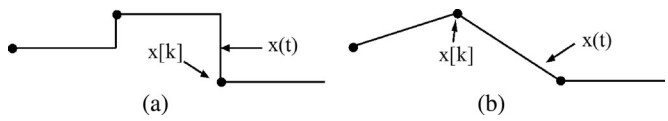

Fig. 3. Comparison of ZOH and triangle-hold. (a) ZOH and (b) triangle-hold.

Then, the following DT equivalent is applied to (24):

$$\begin{aligned} \begin{bmatrix} x_{1,TH,dq}[k+1] \\ x_{2,TH,dq}[k+1] \end{bmatrix} &= \Phi\begin{bmatrix} x_{1,TH,dq}[k] \\ x_{2,TH,dq}[k] \end{bmatrix} + \Gamma\begin{bmatrix} i_{C,dq}[k] \\ v_{g,dq}[k] \end{bmatrix}, \\ \begin{bmatrix} v'_{\mathrm{pcc},dq}[k] \\ i'_{L,dq}[k] \end{bmatrix} &= C\begin{bmatrix} x_{1,TH,dq}[k+1] \\ x_{2,TH,dq}[k+1] \end{bmatrix} + \Lambda\begin{bmatrix} i_{C,dq}[k] \\ v_{g,dq}[k] \end{bmatrix} \end{aligned} \tag{25}$$

where $\Gamma = \Gamma_1 + \Phi\Gamma_2 - \Gamma_2$

$$\begin{bmatrix} \Phi & \Gamma_1 & \Gamma_2 \\ 0_{4\times 4} & I_{4\times 4} & I_{4\times 4} \\ 0_{4\times 4} & 0_{4\times 4} & I_{4\times 4} \end{bmatrix} = e^{\begin{bmatrix} A & B & 0_{4\times 4} \\ 0_{4\times 4} & 0_{4\times 4} & (\frac{1}{T})_{4\times 4} \\ 0_{4\times 4} & 0_{4\times 4} & 0_{4\times 4} \end{bmatrix} T_s}$$

$$\Lambda = D + C\Gamma_2, T_s$$

is the sampling time, and the subscript "TH" has been added to the state variables x and w to indicate that they are not simply sampled versions of $x_{1,dq}$ and $x_{2,dq}$.

The aforementioned transformation, (25), is the so-called triangle-hold equivalent (also called the noncausal, first-order-hold or the slewer-hold) of (22), and the equations are derived in [7, Sec. 6.3.2]. The triangle-hold is the DT equivalent of (22) assuming that the quantities $v_{g,dq}(t)$ and $i_{C,abc}(t)$ are piecewise linear between sampling times [see Fig. 3(b)]. This is in contrast to the more commonly used zero-order-hold (ZOH) equivalent, which assumes that input functions make stepwise transitions [see Fig. 3(a)]. Step changes in $i_{C,abc}(t)$ would lead to very inaccurate results because the system of Fig. 2(b) is highly inductive at the PCC. Instead it is assumed that $i_{C,abc}(t)$ transitions linearly between samples. The decision to use the triangle-hold equivalent is further justified with a discussion in Section III-E and with simulation results in Section V-B.

While this assumption may not be completely accurate for APFs in general, it is a reasonable assumption for multilevel topologies with a high level count such as [12] and [16]. This is because the output current between sampling times has a very low ripple when the number of levels is large enough (see Section III-E).

The term $F\frac{d}{dt} i_{C,dq}$ that was removed for (24) has $F \cdot (i_{C,dq}[k] - i_{C,dq}[k-1])/T_s$ as its triangle-hold equivalent. Therefore, it can be added back to the output expression of (25) to yield

$$\begin{aligned} \begin{bmatrix} v_{\mathrm{pcc},dq}[k] \\ i_{L,dq}[k] \end{bmatrix} &= C\begin{bmatrix} x_{1,TH,dq}[k] \\ x_{2,TH,dq}[k] \end{bmatrix} + \Lambda\begin{bmatrix} i_{C,dq}[k] \\ v_{g,dq}[k] \end{bmatrix} \\ &\quad + \frac{F}{T_s}(i_{C,dq}[k] - i_{C,dq}[k-1]). \end{aligned} \tag{26}$$

Now (26) and (25) are combined to yield the final, open-loop model

$$\begin{bmatrix} x_{1,TH,dq}[k+1] \\ x_{2,TH,dq}[k+1] \\ i_{C,dq}[k] \end{bmatrix} = \Phi' \begin{bmatrix} x_{1,TH,dq}[k] \\ x_{2,TH,dq}[k] \\ i_{C,dq}[k-1] \end{bmatrix} + \Gamma' \begin{bmatrix} i_{C,dq}[k] \\ v_{g,dq}[k] \end{bmatrix}$$

$$\begin{bmatrix} v_{\mathrm{pcc},dq}[k] \\ i_{L,dq}[k] \end{bmatrix} = C' \begin{bmatrix} x_{1,TH,dq}[k] \\ x_{2,TH,dq}[k] \\ i_{C,dq}[k-1] \end{bmatrix} + \Lambda' \begin{bmatrix} i_{C,dq}[k] \\ v_{g,dq}[k] \end{bmatrix} \quad (27)$$

where

$$\Phi' = \begin{bmatrix} \Phi & 0_{4\times 2} \\ 0_{2\times 4} & 0_{2\times 2} \end{bmatrix}, \Gamma' = \begin{bmatrix} \Gamma \\ I_{2\times 2} \end{bmatrix}, C' = \begin{bmatrix} C & -\dfrac{F}{T_s} \end{bmatrix}$$

$$\Lambda' = \left(\Lambda + \begin{bmatrix} \frac{F}{T_s} & 0_{4\times 2} \\ 0_{2\times 2} & 0_{2\times 2} \end{bmatrix} \right),$$

and $i_{C,dq}[k]$ will be derived in the next section.

B. Closed-Loop System Model

To close the loop of Fig. 2, it is first necessary to model the output of the APF with respect to the load current. The APF modeled here will mimic the behavior of the APF in Section II, although it will differ in two ways. The first of these ways is that the reference current determination and the control will be based in the DQ-frame, as shown in Fig. 2(a). As shown later, this will allow the nonlinearity of (7) to be avoided. The second is that it will be controlled in DT. This is because in large APFs (e.g., [12]), it is desirable that the output stage avoid switching losses by using a slow switching speed. Therefore, to maximize the bandwidth of the output current, a deadbeat controller can be used. Described in [18], this type of control is better for implementing in DT. Although the details of such a controller are somewhat complicated, [18] shows that the relationship between the output current and reference current is very simple

$$\begin{bmatrix} I_{C,d}(z) \\ I_{C,q}(z) \end{bmatrix} = \begin{bmatrix} I_{\mathrm{ref},d}(z) \\ I_{\mathrm{ref},q}(z) \end{bmatrix} \frac{1}{z} \quad (28)$$

where $I_{C,dq}$ is the compensator output current in the DQ-frame.

Now a DT reference current identification must be derived that is equivalent to the continuous-time algorithm of (7). Because of (23), instantaneous power flow becomes a function of only the variable i_d. Therefore, real power is proportional to the average value of i_d. Therefore, the equivalent of (5) is very simple in the DQ-frame

$$I_{L,d,\mathrm{est}}(z) = F(z) \cdot I_{L,d}(z) \quad (29)$$

where $F(z) = \frac{z\left(1-e^{-aT_s}\right)}{z-e^{-aT_s}}$ is a first-order, low-pass filter (LPF) and serves the same purpose as F(s) in Fig. 1(b) and (2).

At this point, it should be noted that the APF is working in the same DQ-frame as (27) is implying that the APF's controller has knowledge of the grid voltage angle. This may not be a realistic assumption. However, this assumption need not be the case, as qualified in the next section, in order for the equations derived here to be accurate.

Continuing with the derivation as shown in Fig. 2(b), then, the equivalent of (7) is

$$I_{\mathrm{ref},dq}(z) = I_{L,dq}(z) - \begin{bmatrix} I_{L,d,\mathrm{est}}(z) \\ 0 \end{bmatrix} = \begin{bmatrix} \dfrac{(z-1)e^{-aT_s}}{z-e^{-aT_s}} I_{L,d}(z) \\ I_{L,q}(z) \end{bmatrix}. \quad (30)$$

Then, (28) can be combined with (30) to yield

$$I_{C,dq}(z) = \begin{bmatrix} \dfrac{(z-1)e^{-aT_s}}{z\left(z-e^{-aT_s}\right)} & 0 \\ 0 & \dfrac{1}{z} \end{bmatrix} I_{L,dq}(z). \quad (31)$$

The next step in closing the loop is to write (31) in state-space according to [7, Sec. 4.2.3]

$$\begin{bmatrix} y_1[k+1] \\ y_2[k+1] \\ y_3[k+1] \end{bmatrix} = E \cdot y[k] + H \cdot i_{L,dq}[k], \quad i_{C,dq}[k] = U \cdot y[k] \quad (32)$$

where

$$E = \begin{bmatrix} e^{-aT_s} & 0 & 0 \\ 1 & 0 & 0 \\ 0 & 0 & 0 \end{bmatrix}, H = \begin{bmatrix} 1 & 0 \\ 0 & 0 \\ 0 & 1 \end{bmatrix}$$

and

$$U = \begin{bmatrix} e^{-aT_s} & -e^{-aT_s} & 0 \\ 0 & 0 & 1 \end{bmatrix}.$$

To close the loop, (32) will be combined with (27), the open-loop system. First, however, substitutions are made for the variable $i_{C,dq}$ in (27) and $i_{L,dq}$ in (32) since they will not be driving functions of the closed-loop system

$$\begin{bmatrix} x_{1,TH,dq}[k+1] \\ x_{2,TH,dq}[k+1] \\ i_{C,dq}[k] \end{bmatrix} = \Phi' \begin{bmatrix} x_{1,TH,dq}[k] \\ x_{2,TH,dq}[k] \\ i_{C,dq}[k-1] \end{bmatrix} + \begin{bmatrix} \Gamma'_{\mathrm{left}} & \Gamma'_{\mathrm{right}} \end{bmatrix} \begin{bmatrix} U \cdot y[k] \\ v_{g,dq}[k] \end{bmatrix}$$

$$\begin{bmatrix} v_{\mathrm{pcc},dq}[k] \\ i_{L,dq}[k] \end{bmatrix} = \begin{bmatrix} C'_1 \\ C'_2 \end{bmatrix} \begin{bmatrix} x_{TH,dq}[k] \\ w_{TH,dq}[k] \\ i_{C,dq}[k-1] \end{bmatrix} + \begin{bmatrix} \Lambda'_1 & \Lambda'_3 \\ \Lambda'_2 & \Lambda'_4 \end{bmatrix} \begin{bmatrix} U \cdot y[k] \\ v_{g,dq}[k] \end{bmatrix}$$

$$y[k+1] = E \cdot y[k] + H \times \left(C'_2 \begin{bmatrix} x_{1,TH,dq}[k] \\ x_{2,TH,dq}[k] \\ i_{C,dq}[k-1] \end{bmatrix} + \begin{pmatrix} \Lambda'_2 & \Lambda'_4 \end{pmatrix} \begin{bmatrix} U \cdot y[k] \\ v_{g,dq}[k] \end{bmatrix} \right)$$

$$i_{C,dq}[k] = U \cdot y[k] \quad (33)$$

where $[\,\Gamma'_{\text{left}} \quad \Gamma'_{\text{right}}\,] = \Gamma'$, $\begin{bmatrix} C'_1 \\ C'_2 \end{bmatrix} = C'$, $\begin{bmatrix} \Lambda'_1 & \Lambda'_3 \\ \Lambda'_2 & \Lambda'_4 \end{bmatrix} = \Lambda'$.

Now the two equations can be combined

$$\begin{bmatrix} x_{1,TH,dq}[k+1] \\ x_{2,TH,dq}[k+1] \\ i_{C,dq}[k] \\ y\,[k+1] \end{bmatrix} = \begin{bmatrix} \Phi' & \Gamma'_{\text{left}}U \\ HC'_2 & E + H\Lambda'_2 U \end{bmatrix} \begin{bmatrix} x_{1,TH,dq}[k] \\ x_{2,TH,dq}[k] \\ i_{C,dq}[k-1] \\ y\,[k] \end{bmatrix} + \begin{bmatrix} \Gamma'_{\text{right}} \\ H\Lambda'_4 \end{bmatrix} v_{g,dq}[k]$$

$$v_{\text{pcc},dq}[k] = [\,C'_1 \quad \Lambda'_1 U\,] \begin{bmatrix} x_{1,TH,dq}[k] \\ x_{2,TH,dq}[k] \\ i_{C,dq}[k-1] \\ y\,[k] \end{bmatrix} + \Lambda'_3 v_{g,dq}[k] \tag{34}$$

where the output $i_{L,dq}$ no longer appears as mentioned after (16).

Therefore, after the switch in Fig. 2 closes, the poles of the system are the eigenvalues of $\left[\begin{smallmatrix} \Phi' & \Gamma'_{\text{left}}U \\ HC'_2 & E + H\Lambda'_2 U \end{smallmatrix}\right]$.

It should be noted that in (18) ϕ is aligned with the grid voltage instead of the PCC voltage as is the normal case. It was this key convention that ultimately led to the derivation of an LTI, state-space model because it led to the reference current in (30) being a linear function of the load current. This differs from (7) where the reference current is a nonlinear function of the load current.

C. Remark on the Grid Voltage Reference

In an actual power system, a knowledge of the angle and magnitude of $v_{g,dq}$ may not be available for the DQ-frame controller. Moreover, $v_{g,dq}$ may not be constant due to the action of automatic generator control (AGC). Furthermore, referring the DQ-controller's reference angle to the grid voltage would lead to nonzero real current being injected at the PCC at steady state (because the distinction between real and reactive current is dependent on the angle of V_{pcc}). Therefore, in a practical implementation of Fig. 2, the reference angle used by the DQ-controller will converge on the true angle of the PCC voltage at steady state.

The fact that the DQ-frame's reference angle is not actually stationary does not affect the accuracy of (34) for modeling the rapid transient dynamics as long as the reference angle of the controller is stationary during the transient. In real systems, this should be the case because the reference phase for the DQ-controller should not be sensitive to instantaneous phenomenon such as voltage flicker and harmonics. Therefore, the D and Q components of the grid voltage will remain stationary during the transient.

D. Initial Conditions and Transient Response

In order to use (34) to model the response of system to the closing switch in Fig. 2(a), the initial state of the system needs to be determined at some time after the switch closes. The first step to do this is to define the time frame of the transient response. For the purposes of this analysis, $k = 0$ will be defined as the time at which the switch closes.

The next step is to determine initial voltages and currents in the system. Before the switch closes, there will be no current in the system. Because of the inductors, the load current is zero at the instant the switch closes. Therefore, the compensator current will also be zero

$$i_{C,dq}\,[0] = \begin{bmatrix} 0 \\ 0 \end{bmatrix} \quad i_{L,dq}\,[0] = \begin{bmatrix} 0 \\ 0 \end{bmatrix}. \tag{35}$$

Therefore, at the instant the switch closes, the PCC voltage can be found by ignoring the resistors and applying voltage division across the inductors of Fig. 2(a)

$$v_{\text{pcc},dq}\,[0] = \frac{L_L}{L + L_L} \cdot v_{g,dq}\,[0] = \frac{L_L}{L + L_L} \begin{bmatrix} V_g \\ 0 \end{bmatrix} \tag{36}$$

where $v_{g,dq}\,[0]$ is equal to $\begin{bmatrix} V_g \\ 0 \end{bmatrix}$ due to (20).

One time sample after the switch closes ($k = 1$) the load current will no longer be zero. However, because of the deadbeat delay of the compensator, the compensator current will not respond to the nonzero load current until $k = 2$. Therefore, for the first two time samples ($k = 0$ and 1) of the transient response, the system in Fig. 2(a) is essentially running open loop. Therefore, to model the PCC voltage and load current (during this time only!), the system can be modeled as if the switch was already closed and the grid voltage was suddenly turned on at $k = 0$. Therefore, the well-known, ZOH equivalent is applied to (22) while dropping $i_{C,dq}$ as an input

$$\begin{bmatrix} x_{1,dq}\,[k+1] \\ x_{2,dq}\,[k+1] \end{bmatrix} = \Phi_{\text{Trans}} \begin{bmatrix} x_{1,dq}\,[k] \\ x_{2,dq}\,[k] \end{bmatrix} + \Gamma_{\text{Trans}} \begin{bmatrix} V_g \\ 0 \end{bmatrix}$$

$$\begin{bmatrix} v_{\text{pcc},dq}\,[k] \\ i_{L,dq}\,[k] \end{bmatrix} = C_{\text{Trans}} \begin{bmatrix} x_{1,dq}\,[k] \\ x_{2,dq}\,[k] \end{bmatrix} + \Lambda_{\text{Trans}} \begin{bmatrix} V_g \\ 0 \end{bmatrix} \tag{37}$$

where $k = 0$ or 1, $\Phi_{\text{Trans}} = e^{AT_s}, \Gamma_{\text{Trans}} = A^{-1}(\Phi_{\text{Trans}} - I)\left[\begin{smallmatrix} (a_3)_{2x2} \\ I_{2x2} \end{smallmatrix}\right], C_{\text{Trans}} = C, \Lambda_{\text{Trans}} = \left[\begin{smallmatrix} (a_7)_{2x2} \\ I_{2x2} \end{smallmatrix}\right]$, and $\left[\begin{smallmatrix} x_{1,dq}[0] \\ x_{2,dq}[0] \end{smallmatrix}\right] = (0)_{4x1}$.

The next step is to solve (26) for the initial states of $\left[\begin{smallmatrix} x_{1,TH,dq} \\ x_{2,TH,dq} \end{smallmatrix}\right]$. However, due to the nature of the triangle-hold [which was used to derive (26)], (26) does not become valid until the time sample after the switch closes. Therefore, the initial state of the system will be taken for $k = 1$. Then, according to (26)

$$\begin{bmatrix} x_{1,TH,dq}[1] \\ x_{2,TH,dq}[1] \end{bmatrix} = C^{-1} \left(\begin{bmatrix} v_{\text{pcc},dq}[1] \\ i_{L,dq}[1] \end{bmatrix} - \Lambda \begin{bmatrix} 0 \\ 0 \\ V_g \\ 0 \end{bmatrix} \right). \tag{38}$$

The final step in determining the initial state is to determine the state of the vector $y[1]$. To do this, it is again noted that the load current, $i_{L,dq}[k]$, is zero at and prior to $k = 0$. This fact and the fact that the poles of (32) (eigenvalues of E) are stable mean that the vector y has to be zero at $k = 1$

$$\begin{bmatrix} y_1\,[1] \\ y_2\,[1] \\ y_3\,[1] \end{bmatrix} = \begin{bmatrix} 0 \\ 0 \\ 0 \end{bmatrix}. \tag{39}$$

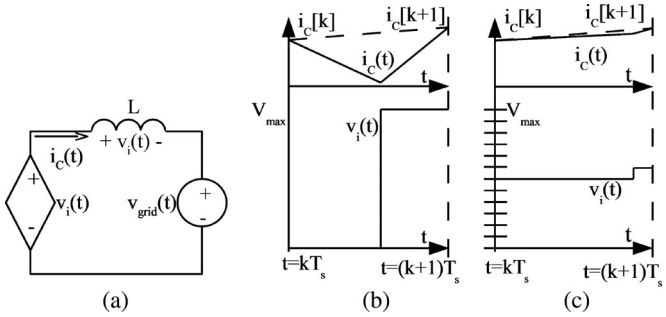

Fig. 4. (a) Simplified illustration of the voltage-source-inverter (VSI)-based current source for each phase of the APF, (b) illustration of how v_i controls i_C when the VSI is three-level, and (c) illustration of how v_i controls i_C for a 25-level VSI.

Equations (35), (38), and (39) can now be combined to yield the initial state:

$$\begin{bmatrix} x_{1,TH,d}[1] \\ x_{1,TH,q}[1] \\ x_{2,TH,d}[1] \\ x_{2,TH,q}[1] \\ i_{C,d}[0] \\ i_{C,q}[0] \\ y_1[1] \\ y_2[1] \\ y_3[1] \end{bmatrix} = \begin{bmatrix} C^{-1}\left(\begin{bmatrix} v_{\mathrm{pcc},dq}[1] \\ i_{L,dq}[1] \end{bmatrix} - \Lambda \begin{bmatrix} 0 \\ 0 \\ V_g \\ 0 \end{bmatrix} \right) \\ 0 \\ 0 \\ 0 \\ 0 \\ 0 \end{bmatrix}. \tag{40}$$

where $v_{\mathrm{pcc},dq}$ and $i_{L,dq}$ at $k=1$ are given by (37).

However, this means that (34) cannot be used to calculate the response of $v_{\mathrm{pcc},dq}$ at $k=0$. That is fine because $v_{\mathrm{pcc},dq}[0]$ is given by (36).

E. Discussion of Appropriate Hold

In order to derive a DT equivalent of the system in Fig. 2(a) with respect to i_C as an input, it necessary to make some assumptions about the continuous-time (CT) trajectory of i_C between sampling times. In order to do this, it is necessary to consider how the current is synthesized. This is illustrated in Fig. 4.

In Fig. 4(a), i_C flows from the inverter through an inductor to the PCC of the grid. The inverter voltage, v_i, works with the PCC voltage (which is assumed to be an infinite bus and constant over a time sample for the purposes of current control) to control the voltage across the inductor, v_L, so that i_C is controlled correctly. In the case of a conventional inverter, three-level pulse-width-modulation is used to control the average value of v_L over each time sample so that i_C will transition from $i_C[k]$ to $i_C[k+1]$, as shown in Fig. 4(b) [the third voltage level is not shown in Fig. 4(b) because it is negative $V_{\max}$]. In order to achieve the deadbeat control of (28), $i_C[k+1]$ is set equal $i_{\mathrm{ref}}[k]$ and $v_i[k]$ is calculated accordingly.

For reasons given in [12] and [16], it is unlikely that a three-level inverter will be used for the charging station/APF. Rather, it is likely that a DT-controlled, multilevel inverter with a high level count (hereafter referred to as a "next-generation grid interface") will be used. Illustrated in Fig. 4(c) for a 25-level inverter (only 13 voltage level choices are shown because the remaining levels are negative), the control of i_C is very similar in principle to the three-level case, except that multilevel PWM is used. As shown in Fig. 4(c), this means that v_i and, therefore, v_L are more nearly constant over the sample time. Therefore, the slope of i_C is nearly constant as it transitions from $i_C[k]$ to the reference current($i_C[k+1]=i_{\mathrm{ref}}[k]$) one sample time later.

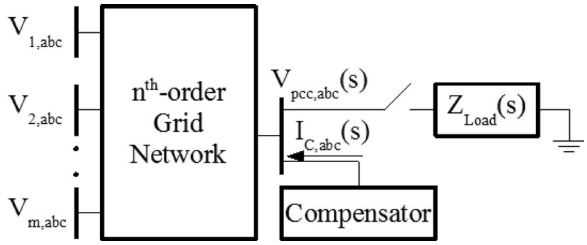

Fig. 5. Generalized APF integrated into a generalized power system.

Obviously, a ZOH would be a poor way to model the CT transitions of the current between sampling times because the current does not have step changes. Additionally, for i_C as an input to the network in Fig. 2(a), a ZOH equivalent would be mathematically meaningless because of the inductors L and L_L. Because there are no step changes in i_C and because there is a delay between i_C and i_{ref}, a natural choice to model i_c is a ZOH followed by the smoothing filter $\frac{1/T_s}{s+1/T_s}$, which is chosen because it has a group delay of T_s for low frequencies. However, this approach, which will be referred to as ZOH+LPF, leads to i_C changing slope over the course of each sample time. Furthermore, due to the changing slope, the current i_C will not fully transition to the reference current by the end of the sampling time (demonstrated with simulation in Section V-B).

It is much more accurate to assume that i_C transitions linearly from $i_C[k]$ to $i_C[k+1]$ [dotted line in Fig. 4(c)]. This is known as the triangle-hold. Therefore, the triangle-hold equivalent is applied in (24)–(27). It is much more accurate than using a ZOH+LPF and is no more complicated [the triangle-hold equivalent yields a six-state model in (27) as would the ZOH+LPF approach]. In Section V-B, simulation is used to verify that a unit-delayed, triangle hold is an accurate output current with respect to the reference current when a next generation grid interface is used. The simulation results will also show that the ZOH+LPF approach is much less accurate.

IV. Procedure and Equations in the General Case

A. Generalized Procedure for Deriving a Linear, Closed Loop

1) Write the state-space description of the open-loop system in Fig. 5:

$$\dot{x}_{3n\times 1}(t) = J\cdot x_{3n\times 1}(t) + \sum_{x=1}^{m} K_x \cdot v_{x,abc}(t) + K_{m+1}\cdot i_{C,abc}(t),$$

$$\begin{bmatrix} v_{\mathrm{pcc},abc}(t) \\ i_{L,abc}(t) \end{bmatrix} = L\cdot x_{3n\times 1}(t) + \sum_{x=1}^{m} M_x \cdot v_{x,abc}(t) + M_{m+1}\cdot i_{C,abc}(t) + M_{m+2}\cdot\left(\frac{d}{dt} i_{C,abc}(t)\right). \tag{41}$$

where $\dot{x}_{3nx1}(t)$ is the state column of length $3n$ (number of phases times order of system), m is the number of sources in Fig. 5, and J, K_x, L, and M are based on knowledge of the system. For the simple case in (17), the state variable consisted of $x_{1,abc}$ and $x_{2,abc}$. According to the nomenclature of this section, that would correspond to $x_{6\times1}(t)$, and n would equal 2.

2) Transform (41) into the DQ-frame according to the procedure discussed in [9, Ch. 3] and referring the angle of the DQ-transform to the angle of the PCC voltage prior to the transient:

$$\dot{x}_{dq}(t) = J_{dq}\cdot x_{dq}(t) + [K_{1,dq},\ldots,K_{m+1,dq}]\begin{bmatrix} v_{1,dq} \\ \vdots \\ v_{m,dq} \\ i_{C,dq}\end{bmatrix},$$

$$\begin{bmatrix} v_{\mathrm{pcc},dq}(t) \\ i_{L,dq}(t)\end{bmatrix} = L_{dq}\cdot x_{dq}(t) + [M_{1,dq},\ldots,M_{m+1,dq}] \times \begin{bmatrix} v_{1,dq} \\ \vdots \\ v_{m,dq} \\ i_{C,dq}\end{bmatrix} + M_{m+2,dq}\cdot\left(\frac{d}{dt}i_{C,dq}(t)\right) \quad (42)$$

where $J_{dq}, K_{1\sim m}, L$, and M are constant if (41) represents a balanced system. If this is not the case, this method will still linearize the loop, but the parameters J_{dq}, K_x, L, and M will become functions of time. Therefore, if the system is unbalanced, (41) should be decomposed into symmetrical components in Step 1.

3) Transform (42) into DT using the triangle-hold equivalent [7]:

$$x_{TH}[k+1] = \Pi'\cdot x_{TH}[k] + [\Delta'_1,\ldots,\Delta'_{m+1}]\begin{bmatrix} v_{1,dq} \\ \vdots \\ v_{m,dq} \\ i_{C,dq}\end{bmatrix}$$

$$\begin{bmatrix} v_{\mathrm{pcc},dq}[k] \\ i_{L,dq}[k]\end{bmatrix} = L'_{dq}\cdot x_{TH}[k] + [\Omega'_1,\ldots,\Omega'_{m+1}]\begin{bmatrix} v_{1,dq} \\ \vdots \\ v_{m,dq} \\ i_{C,dq}\end{bmatrix} \quad (43)$$

where

$$\Pi' = \begin{bmatrix}\Pi & 0_{2n\times2} \\ 0_{2\times2n} & 0_{2\times2}\end{bmatrix}, \Delta_{1\sim m} = \begin{bmatrix}\Gamma_{1\sim m,1} + \Pi\cdot\Gamma_{1\sim m,2} - \Gamma_{1\sim m,2} \\ 0_{2\times2}\end{bmatrix}$$

$$\Delta'_{m+1} = \begin{bmatrix}\Gamma_{m+1,1} + \Pi\cdot\Gamma_{m+,2} - \Gamma_{m+1,2} \\ I_{2\times2}\end{bmatrix}, \begin{bmatrix}\Pi & \Gamma_{x,1} & \Gamma_{x,2} \\ [0] & I & I \\ [0] & [0] & I\end{bmatrix}$$

$$= e^{\begin{bmatrix} J_{dq} & K_x & [0] \\ [0] & [0] & [1/T_s] \\ [0] & [0] & [0]\end{bmatrix}\cdot T_s}, L'_{dq} = [L_{dq}, -M_{m+2,dq}], \Omega'_{1\sim m}$$

$$= M_{1\sim m,dq} + L_{dq}\Gamma_{1\sim m,2}, \Omega'_{m+1}$$

$$= M_{m+2,dq} + M_{m+1,dq} + L_{dq}\Gamma_{m+1,2}$$

and T_s is the sampling time.

4) Derive the state-space relationship of $i_{L,dq}$ and $i_{C,dq}$ according to the APF in Fig. 5:

$$w[k+1] = N\cdot w[k] + P\cdot i_{L,dq}[k], \quad i_{C,dq}[k] = Q\cdot w[k] \quad (44)$$

where N, P, and Q are based on knowledge of the compensator. In (29) the low-pass filter, $F(z)$, and the APF dynamics, $C(z)$, were very specific. This time N, P, Q, and R are left open to allow for a general case APF.

5) Close the loop by combining (43) and (44):

$$\begin{bmatrix} x_{TH}[k+1] \\ w[k+1]\end{bmatrix} = \begin{bmatrix}\Pi' & \Delta'_{m+1}Q \\ PL_2 & N + P\Omega'_{2,m+1}Q\end{bmatrix}\begin{bmatrix} x_{TH}[k] \\ w[k]\end{bmatrix} + \begin{bmatrix}[\,\Delta'_1,\cdots,\Delta'_m\,] \\ P\cdot[\,\Omega'_{2,1},\cdots\Omega'_{2,m}\,]\end{bmatrix}\cdot\begin{bmatrix} v_{1,dq} \\ \vdots \\ v_{m,dq}\end{bmatrix}$$

$$v_{\mathrm{pcc},dq}[k] = [\,L_1 \quad \Omega'_{1,m+1}\cdot Q\,]\begin{bmatrix} x_{TH}[k] \\ w[k]\end{bmatrix} + [\,\Omega'_{1,1},\cdots\Omega'_{1,m}\,]\begin{bmatrix} V_{1,dq} \\ \vdots \\ V_{m,dq}\end{bmatrix} \quad (45)$$

where $\begin{bmatrix}\Omega'_{1,1},\ldots\ \Omega'_{1,m+1} \\ \Omega'_{2,1},\ldots\ \Omega'_{2,m+1}\end{bmatrix} = [\,\Omega'_1,\ldots\ \Omega'_{m+1}\,], \begin{bmatrix} L_1 \\ L_2\end{bmatrix} = L'_{dq}$, and the output $i_{L,dq}$ no longer appears as happened in (34).

B. Initial Conditions in the General Case Transient Response

In the simple case, the length of the output of (26) has the same length as the number of states. Therefore, (26) can be solved for the state vector because C can be inverted. This is not usually the case with the generalized approach because (41) can have fewer outputs than states. Therefore, (41) needs to be modified with a new output vector that is equal in length to the state vector. Since the three-phase system of (41) has $3n$ states, there should be n, three-phase, linearly independent quantities (either voltage and/or currents) that are physically observable. The important thing about these quantities is that they provide additional, linearly independent pieces of information and can be easily determined after the load transient based on fundamental network theory. This new output vector, which includes the outputs already in (41), is called out_{abc}, and modifies (41)

$$\mathrm{out}_{abc}(t) = \begin{bmatrix} v_{\mathrm{pcc},abc}(t) \\ i_{L,abc}(t) \\ \mathrm{out}_{3,abc}(t) \\ \vdots \\ \mathrm{out}_{n,abc}(t)\end{bmatrix} = L_{\mathrm{mod}}\cdot x_{3nx1}(t) + \sum_{x=1}^{m} M_{\mathrm{mod},x}\cdot v_{x,abc}(t) + M_{\mathrm{mod},m+1}\cdot i_{C,abc}(t) + M_{\mathrm{mod},m+2}\cdot\frac{d}{dt}i_{C,abc}(t) \quad (46)$$

where L_{mod} and M_{mod} contain L and M, respectively, from (41), as well as additional rows to make their row count equal to $\mathrm{out}_{abc}(t)$.

In the aforementioned equation, the additional rows added to form L_{mod} and M_{mod} are based on knowledge necessary to create the additional observable outputs. Likewise, the output expression of (42) is modified

$$\mathrm{out}_{dq}(t) = \begin{bmatrix} v_{\mathrm{pcc},dq}(t) \\ \vdots \\ \mathrm{out}_{n,dq}(t) \end{bmatrix} = L_{\mathrm{mod},dq} \cdot x_{dq}(t) + [\, M_{\mathrm{mod},1,dq}, \ldots, M_{\mathrm{mod},m+2,dq} \,] \begin{bmatrix} v_{1,dq}(t) \\ \vdots \\ v_{m,dq}(t) \\ i_{C,dq}(t) \\ \dfrac{d}{dt} i_{C,dq}(t) \end{bmatrix} \quad (47)$$

where the procedure of [7, Ch. 3] is used to transform L_{mod} and M_{mod} into $L_{\mathrm{mod},dq}$ and $M_{\mathrm{mod},dq}$.

Then, the final step to derive an analog of (38) for the general case is to modify the output expression of (43)

$$\mathrm{out}_{dq}[k] = L'_{\mathrm{mod},dq} \cdot x_{TH}[k] + \Omega'_{\mathrm{mod}} \begin{bmatrix} v_{1,dq}[k] \\ \vdots \\ i_{C,dq}[k] \end{bmatrix}$$

where $L'_{\mathrm{mod},dq} = [\, L_{\mathrm{mod},dq}, \quad -M_{\mathrm{mod},m+2,dq} \,]$ and $\Omega'_{\mathrm{mod}} = [\, M_{\mathrm{mod},\,1\sim m,dq} + L_{\mathrm{mod},\,dq} \cdot \Gamma_{1\sim m,2}, \quad M_{\mathrm{mod},m+2,dq} + M_{\mathrm{mod},m+1,dq} + L_{\mathrm{mod},dq} \cdot \Gamma_{m+1,2}]$, and to solve for $x_{TH}[1]$:

$$x_{TH}[1] = L'^{-1}_{\mathrm{mod},dq} \cdot \mathrm{out}_{dq}[1] - \Omega'_{\mathrm{mod}} \begin{bmatrix} v_{1,dq}[1] \\ \vdots \\ i_{C,dq}[1] \end{bmatrix}. \quad (48)$$

In order for (48) to be used, the state of the compensator at $k = 1$ must be determined. In this case, it cannot be assumed that load current is zero prior to the transient because there may have already been a load present prior to the transient. However, except in rare cases where the load transient results in a step in load current, the compensator state, $w[k]$, will not be affected by the load transient until $k = 2$. This is because, according to (44), $w[k]$ is a function of the previous value of the load current, $i_{L,dq}[k–1]$. Under these circumstances, $i_{C,dq}[1]$ can be calculated as if the load has not been connected. Therefore, the final expression for the initial state is

$$\begin{bmatrix} x_{TH}[1] \\ w[1] \end{bmatrix} = \begin{bmatrix} L'^{-1}_{\mathrm{mod},dq} \cdot \left(\mathrm{out}_{dq}[1] - \Omega'_{\mathrm{mod}} \begin{bmatrix} v_{1,dq}[1] \\ \vdots \\ i_{C,dq}[1] \end{bmatrix} \right) \\ w[1] \end{bmatrix} \quad (49)$$

where the state of the compensator $w[1]$ and the compensator output $i_{C,dq}[1]$ are determined by assuming that the load has not been connected and the chosen observable output states $\mathrm{out}_{dq}[1]$ are solved for based on knowledge of the circuit and the chosen states.

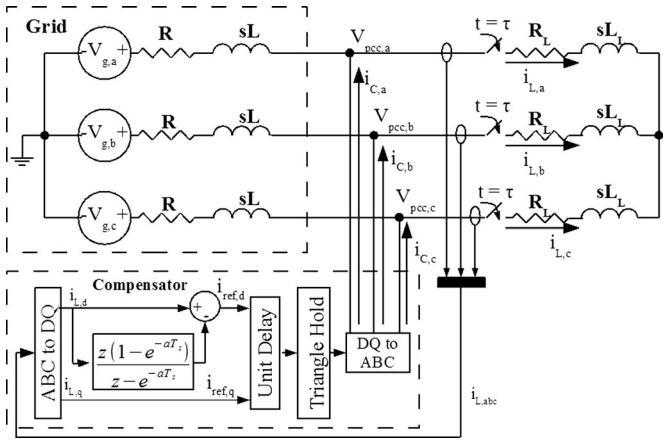

Fig. 6. Block diagram of the simulated system. The "ABC to DQ" block uses (21) and the "DQ to ABC" is an ideal current source that converts its DQ-frame input signal into an ABC-frame current. The "unit delay" and "triangle-hold" are shown as two separate mathematical operations although, in simulation they cannot be separated this way because a triangle-hold by itself is noncausal [see Fig. 7(b)].

V. Simulation Verification

A. Verification of the Derived Model

To verify the transient response models developed in Sections IV and V, the system in Fig. 6 was simulated with the SimPowerSystems package of Simulink. This simulation was performed for four scenarios. For the different scenarios, the parameters are specified in Table I. In addition, for all scenarios there is no load present prior to the switch closing. To implement the compensator as modeled in (34), the compensator model shown in Fig. 6 was used. Then, the PCC voltage of the simulations was observed and converted into the DQ-frame. All ABC-to-DQ and DQ-to-ABC transformations use the conventions of (21).

Table I also describes each scenario in practically meaningful terms. This is done in the comments column which describes how "strong" the line is and how "heavy" the load is for each scenario. For scenarios 1 and 3, the term "typical dist. line" means that R_{line} and L_{line} have been chosen such that the X/R ratio is 5, and a 1-MW load causes a very small voltage drop. In contrast, scenario 2 is described as a "weak line" because X/R $= \infty$ and the impedance is several times greater than the typical line.

The Simulink model used for the simulation is shown in Fig. 7(a). Of particular interest is the subsystem TH, which implements the unit-delayed triangle-hold. In Fig. 6, this was shown as two separate mathematical operations. In simulation (and in any physical system) these two operations cannot be separated this way because, by itself, the triangle-hold is a noncausal operation. Therefore, the unit-delayed triangle-hold is implemented by the set of operations in Fig. 7(b). Also, (45) and (49) are implemented by the blocks "mathematically derived model state" and "output observer." Since the network model has a relay that closes at $t = \tau$, the output of the mathematical blocks is delayed. The initial state of the "mathematically derived model state" block is determined by (49). The purpose

TABLE I
DESCRIPTION OF THE SIMULATION IN FIG. 7

Scenario	Parameters	Plot in Figs. 7 and 8	Comments
1	R_{line}=0.06 Ω, L_{line}=796 μH R_{load}=22.8 Ω, L_{load}=6.1 mH	a	1 MW +0.1 MVAR, 0.4 % Steady State Volt. Drop, Typical Dist. Line
2	R_{line}=0 Ω, L_{line}=2.65 mH R_{load}=4.61 Ω, L_{load}=0 H	b	5 MW, 2.2% Steady State Volt. Drop, Heavy Transient on Weak Line
3	R_{line}=0.06 Ω, L_{line}=796 μH R_{load}=11.5 Ω, L_{load}=31 mH	c	1 MW + 0.1 MVAR, .8% Steady State Volt. Drop, Med. Trans on Typ. Line
4	R_{line}=.06 Ω, L_{line}=796 μH R_{load}=0 Ω, L_{load}=61 mH	d	14 MVAR, 11% Steady State Volt. Drop, Heavy, undamped Transient

All Scenarios			
Parameter	Value	Parameter	Value
Grid Voltage	4800 $V_{RMS,line-line}$, 60 Hz	Time constant of F(z)	a=0.1 sec
Switch Closing	τ=0.1 sec	Sample Rate	4320 Hz
Results	Exact match between modeled and simulated quantities at discrete sampling times.		

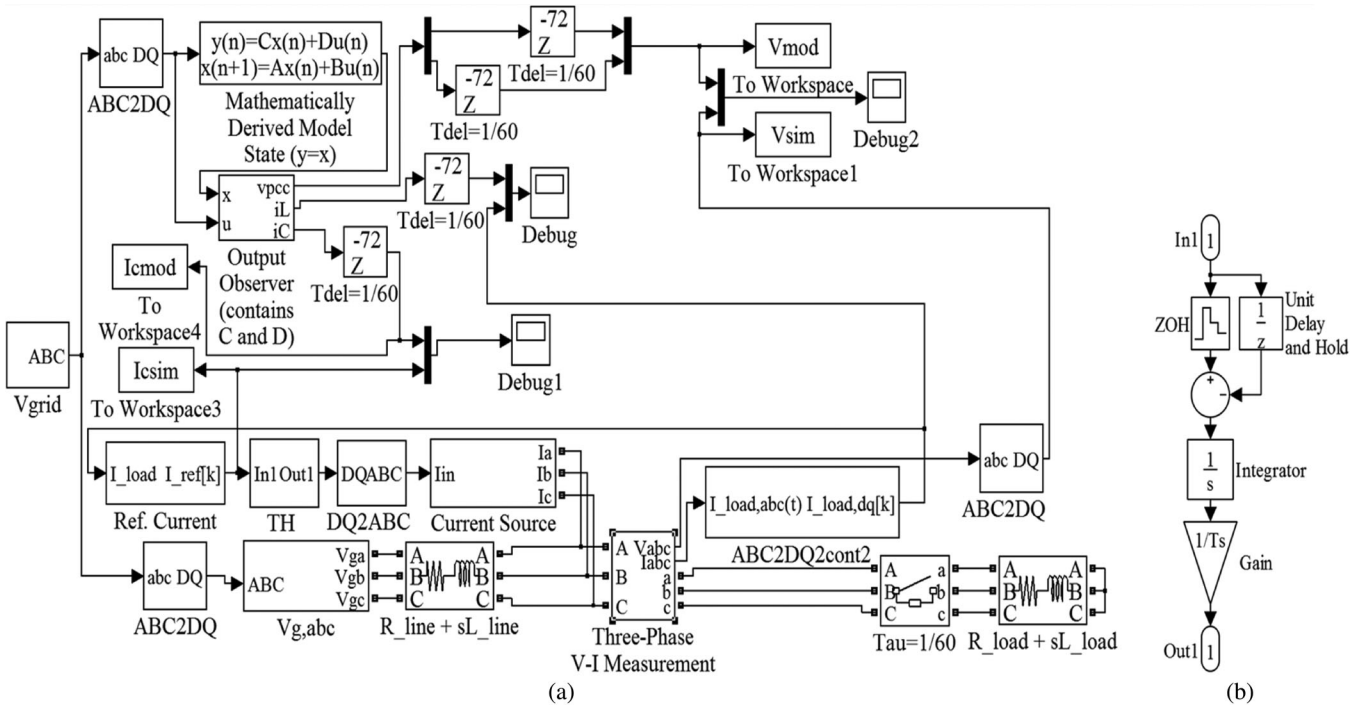

Fig. 7. (a) Simulink model capture for scenarios 1–4. Of particular interest is the TH block which forces the compensator current to be a unit-delayed, triangle-held version of the reference current. (b) TH block model.

of the "to workspace" blocks is to pass the observed simulation and mathematical results to the MATLAB environment so that Figs. 8 and 9 could be generated.

Each scenario in Table I was also modeled according to (34), the derived closed-loop, DT, DQ-frame model. In accordance with Section III-D, (36) was used to calculate the PCC voltage at the time of the transient ($k = 0$). Then, (40) was used to calculate the system state at $k = 1$ in order for (34) to be used for subsequent values of k. The parameters used for the equation were based on a sampling rate of 4320 Hz, V_g of 3919 V (the peak magnitude corresponding to 4800 $V_{\mathrm{RMS,phase\text{-}phase}}$), an ω_g of 2π60/s, and an a [from (29)] of 10/s, and the parameters specified in Table I. Then, for each scenario, the PCC voltage generated by the model is compared to the simulated PCC voltage in Fig. 9 in the DQ-frame.

Fig. 8 shows the mathematically modeled compensator current, $i_{C,dq}[k]$, [produced by advancing the state-variable $i_{C,dq}[k-1]$ in (34)]. Since this is a DT quantity, $i_{C,dq}$ for each value of k is indicated with an "x." Since (27) was derived by assuming that the continuous compensator current $i_{C,dq}(t)$ is linear

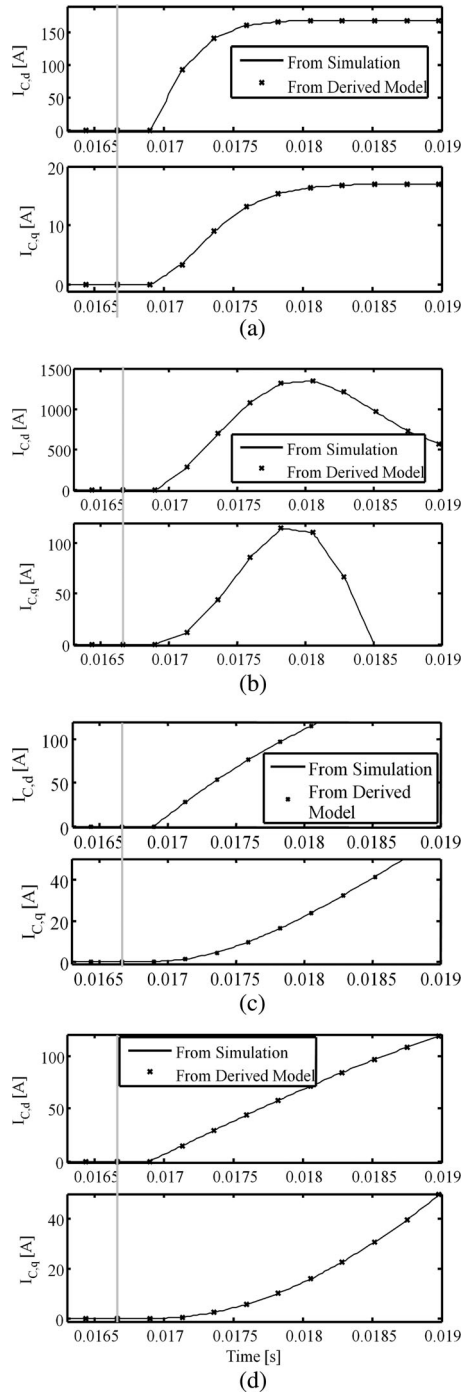

Fig. 8. Mathematically modeled (solid trace) compensator current in the DQ-frame compared to the simulated voltage for the four different scenarios listed in Table I. Note the vertical, gray line in each plot at $t = 0.0167$ indicates the closing of the switch in Fig. 2(a).

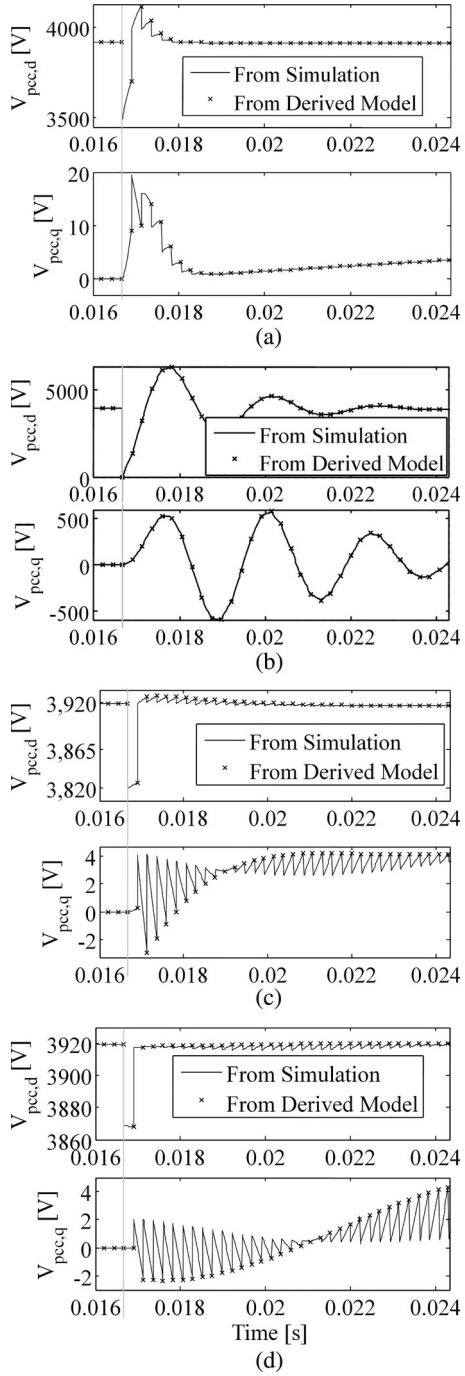

Fig. 9. Mathematically modeled (solid trace) PCC voltage in the DQ-frame compared to the simulated voltage for the four different scenarios listed in Table I. Since the model is in DT, it perfectly matches the simulated voltage at the end of each sample time. The vertical, gray line in each plot at $t = 0.0167$ indicates the closing of the switch in Fig. 2(a).

between sampling times, this was enforced in the simulation. This is also shown in Fig. 8 because the simulated current (solid trace) connects the DT current with perfectly straight segments.

As Fig. 9 shows, the continuous-time PCC voltage of the physical model corresponds exactly with the output of the mathematical model at discrete sampling times. In between sampling times, however, the continuous-time voltage may exhibit significant ripple. This is because the triangle-hold assumed for (27) applies only to the inputs of system (which were $v_{g,dq}$ and $i_{C,dq}$). It does not imply any nature to the intra-sample trajectory of output quantities. If this level of detail in the derived model is required, the reader is referred to [7, Sec. 5.5].

The exact correspondence between simulated and modeled quantities (at sampling times) in Figs. 9 and 10 verifies two things. The first thing it verifies is the derived procedure to

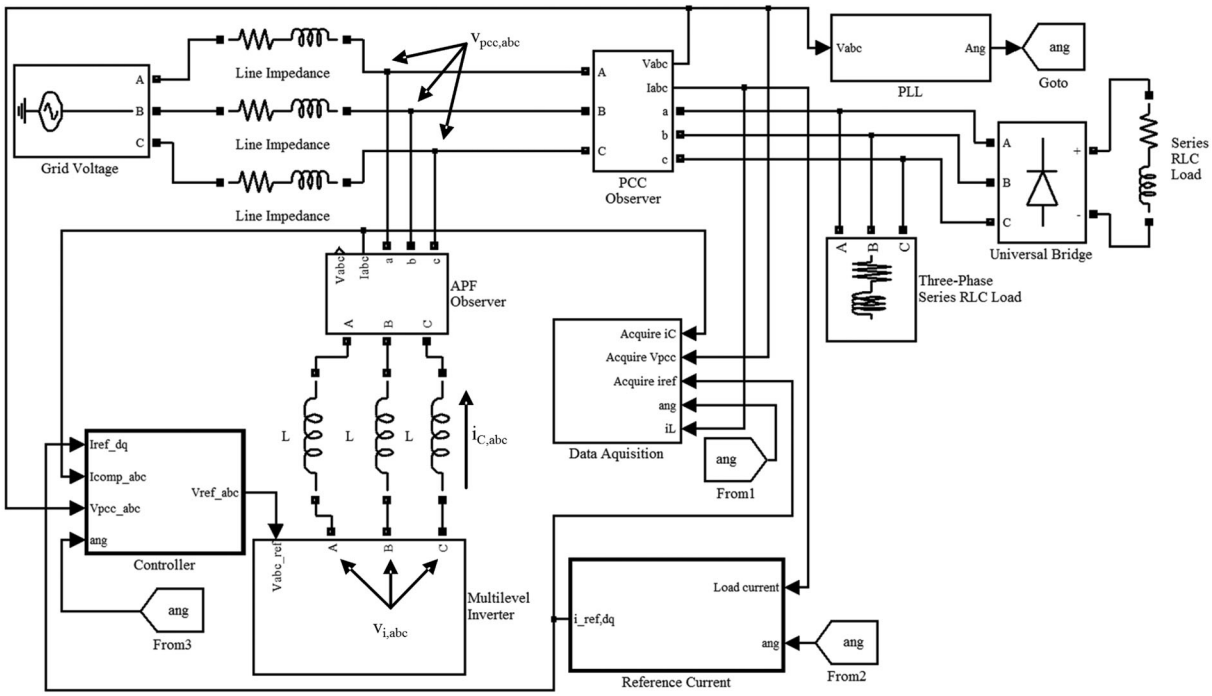

Fig. 10. Capture of Simulink model to simulate a practical APF. It is similar to the previous simulations except that the effects of a phase-locked loop (PLL), a harmonic load, and a nonideal current source are modeled. The APF and PCC observer blocks measure current and, therefore, have zero throughput impedance. Also, labels have been added for the quantities $v_{i,abc}$, $i_{C,abc}$, and $v_{\mathrm{pcc},abc}$ to provide context for (50).

TABLE II
SIMULATION PARAMETERS

Parameter	Value	Parameter	Value
Load Power	1.90 MW+0.20 MVAR, balanced	Control System Sample Rate	4320 Hz
Load THD	13.8 %	Phase-Locked-Loop (PLL) time constant	0.1 sec.
Line Impedance	0.06 Ω + j0.3 Ω	ABC to DQ Transformation	Eq. 21
Grid Voltage	4800 $V_{L\text{-}L,RMS}$	DQ to ABC Transformation	Eq. 21
Reference Current	Eq. 29 with 0.1 sec. time constant	Multi-level Inverter Output Voltage Step Size	333 V

determine the transient response. More importantly, the second thing it verifies is the correctness of the poles of (34) which can be used to directly determine stability, stability margins, settling time, etc.

B. Verification of Assumptions With a Practical Simulation

The validity of the five-step procedure of Section IV hinges on two very important assumptions regarding the output current of the APF. The first is that the output current is triangle-held between sampling times. The second is that the output current, i_C, is only a function of the load current, i_L. This section will validate the first assumption. Regarding the second assumption, this section will show that, at sample times, i_C is equal to the DT reference current of the previous sample (i.e., deadbeat control can be achieved). Therefore, i_C can be decoupled from other states of the system, validating (44).

Fig. 10 shows a SimPowerSystems model of an APF connected to a simple grid with an active, reactive, and harmonic load. In contrast to the previous simulations, this simulation does not use ideal current sources for the APF. Instead it models the current source for each phase as a cascaded, multilevel inverter in series with an inductor which is how the "next-generation" grid interface will work. The system specifications are given in Table II. Also, the dc-link voltage of the multilevel inverter is 333 V and the multilevel PWM is synchronized with the DT controller, i.e., there is a 333 V rising or falling edge in each phase of the inverter voltage every 4320th of a second. Also, DQ-transformations are performed in the reference current, controller, and data acquisition blocks according to (21).

To achieve deadbeat control of current, the controller in Fig. 10 looks at the difference between output (i_C) and reference currents (i_{ref}) at the beginning of each sample and calculates the voltage necessary to apply across the inductors, L, in order to make the error converge to zero at the end of the sample. This is done in accordance with [18], which derives the following relationship between i_C, v_i, and v_{pcc} in the DQ-frame:

$$\frac{d}{dt}\left(i_{C,dq}\right) = \begin{bmatrix} 0 & -\omega \\ \omega & 0 \end{bmatrix} i_{C,dq} + \frac{1}{L}\left(v_{i,dq} - v_{\mathrm{pcc},dq}\right) \quad (50)$$

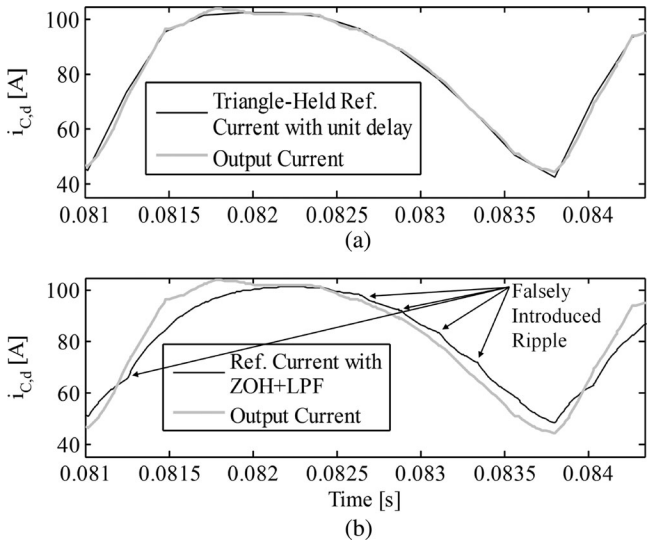

Fig. 11. Output current of compensator, i_C, (a) compared to the reference with unit-delayed triangle-hold and (b) compared to the reference current with a ZOH+LPF.

where

$$i_{C,dq} = T_{dq} \cdot i_{C,abc}, v_{i,dq} = T_{dq} \cdot v_{i,abc}, v_{\mathrm{pcc},dq} = T_{dq} \cdot v_{\mathrm{pcc},abc},$$

$$T_{dq} = \begin{bmatrix} \cos(\omega t) & \cos(\omega t - 2\pi/3) & \cos(\omega t + 2\pi/3) \\ \sin(\omega t) & \sin(\omega t - 2\pi/3) & \sin(\omega t + 2\pi/3) \end{bmatrix}.$$

From this point, [18] shows that the appropriate inverter voltage to achieve deadbeat control is

$$v_{i,dq}[k] = v_{\mathrm{pcc},dq}[k] + \Gamma^{-1}\left(I_{\mathrm{ref}}[k] - \Phi i_{C,dq}[k]\right). \quad (51)$$

where $\Phi = e^{\begin{bmatrix} 0 & -\omega \\ \omega & 0 \end{bmatrix} T_s}$, $\Gamma = \begin{bmatrix} 0 & -\omega \\ \omega & 0 \end{bmatrix}^{-1} (\Phi - I)/L$, and T_s is the sampling time.

This voltage is then transformed back into the ABC-frame (inside the controller block) and fed as a three-phase reference to the multilevel inverter block. The multilevel inverter block then synthesizes this voltage using per-phase, multilevel, regular sampled (at 4320 Hz) PWM.

In Fig. 11(a), the D-component of the output current, i_C, is shown (gray trace). Section III-E argues that the output current is accurately modeled by applying a unit-delayed, triangle-hold to the reference current. Therefore, in the same graph the reference current has been plotted with a unit-delayed triangle-hold (black trace). Section III-E also theoretically explains the ZOH+LPH approach but argues that it is a less accurate model of the output current. Therefore, this model has been compared to the output current as well in Fig. 11(b).

The results shown in Fig. 11(a) confirm that i_C makes relatively linear transitions between sampling times and that it follows the unit-delayed reference current closely. Therefore, when deadbeat control (51) is used with a "next-generation" topology, it is very reasonable to model i_C as a unit-delayed, triangle-held version of the reference current. Therefore, the triangle-hold equivalent is an appropriate way to derive a DT-equivalent. Fig. 11(b), however, shows that applying a ZOH+LPF to the reference current is an inferior model of i_C. While the ZOH+LPF modeled current (black trace) does smoothly *approximate* the actual i_C (gray trace), the black trace follows the gray trace much more closely in Fig. 11(a). In addition, there are ripples in the ZOH+LPF modeled current (black trace) in Fig. 11(b) that are not in the actual i_C. These artifacts are not present in the triangle-hold model [see Fig. 11(a)]. Therefore, even if the input of the ZOH+LPF could be modified so that gray and black traces matched at sampling times, the ripples would still be present. Therefore, assuming that i_C can be modeled by applying a ZOH+LPF to the reference current will not lead to an accurate DT-equivalent.

VI. Proposed Experiment Setup

Experimental results are not currently available. This is because the research reported herein is part of a multiyear, concept-to-prototype project that has not yet reached the hardware stage. Forthcoming results will be reported in future publications. Thus, only a proposal for experimental verification is made. However, the simulations in the previous section were very thorough for that reason. Four scenarios were simulated, and the mathematical model yielded by the five-step procedure was validated for each one. Also, a second simulation was performed that validated the assumption that the compensator current can be modeled by a delayed triangle-hold. In that second simulation, the effects of the multilevel inverter ("next-generation" topology), the effects of grid impedance, the dynamics of an actual phase-locked loop (PLL), and the effects of a harmonic load were all simulated.

For verification purposes, the network and APF in Fig. 10 can be constructed according to the parameters given in Table II. For the multilevel inverter of the APF, the topology of [12] will be used, which consists of 12, cascaded H-bridges per phase. For the reference current identification (29) will be used, and (51) will be used to control the current. To modulate the multilevel inverter so that the reference voltage is correctly synthesized, the multilevel space vector PWM approach described in [8] can be used. The DQ-Frame will be defined in accordance with (21), circumventing the need for the PLL block. Finally, the harmonic load (Universal Bridge/Series RLC Load in Fig. 10) will be realized with an independent current source (using the same topology as the APF).

VII. Conclusion

This paper examines a nonlinear, closed loop that is created when grid-connected power electronics using instantaneous power-based controllers interact with the grid's Thevenin impedance Z_{Th} (Fig. 1). This is of particular concern because the presence of such devices is expected to increase in the form of large EV charging stations, APFs, distributed generation, distributed storage, etc. In the case of APFs, additional, closed-loop dynamics are introduced that are rapid in nature. The nonlinear, closed loop makes it very difficult to analyze these dynamics and, prior to the publication of the conference paper [19] on which this paper is based, no suitable method had been published to determine the stability, settling time, etc. of these dynamics.

The first contribution of this paper is that it transforms the nonlinear, closed loop into an LTI, closed loop. It uses DQ-theory to do this. This is first done for a simple, DT-controlled

APF connected to a simple power system, yielding a set of LTI difference equations whose stability and transient response can easily be determined. This method is then generalized as a straightforward procedure that yields LTI difference equations for a general class of DT-controlled APFs. Furthermore, the procedure can be easily applied to a wide variety of APFs (any APF whose output current is an LTI function of the load current) connected to any power system that can be modeled as an admittance network. It is finally validated in Simulink for a simple scenario.

This paper does not indicate how to achieve or improve the stability of a grid-connected APF if the closed-loop transient response or poles [characteristic values of (34) and (45)] are not found to be suitably stable. It only provides a straight-forward way in which to derive an LTI model for a given closed loop. However, it is the authors' intention that this will provide a framework in which design choices can be made to improve stability and transient response. In particular, there is a lot of design flexibility in the algorithms used by an online controller to identify the reference current and to make the output current follow it. In order to allow the five-step procedure to be very accommodating of such design choices, step four of the modeling procedure is very open in terms of compensator design decisions.

The second contribution of this paper is its novel use of the triangle-hold to model the output current of "next-generation" (as described in Section III-E) grid interfaces. The triangle-hold equivalent was used so that an accurate DT-equivalent could be derived for the fourth step of the aforementioned, five-step procedure. However, modeling the output current of a next generation grid interface with a triangle-hold has applications beyond modeling a grid-connected APF. Grid interaction can be more accurately modeled in DT in other medium-voltage, high-power applications such as distributed generation, STATCOMs because, as shown in Sections III-E and V-B, a wide variety of next-generation grid interfaces will have output current that is well modeled by the triangle-hold.

REFERENCES

[1] W. Shireen and L. Tao, "A DSP-based active power filter for low voltage distribution systems," *Electr. Power Syst. Res.*, vol. 78, pp. 1561–1567, Sep. 2008.

[2] V. Khadkikar, "Enhancing electric power quality using UPQC: A comprehensive overview," *IEEE Trans. Power Electron.*, vol. 27, no. 5, pp. 2284–2297, May 2012.

[3] P. Kundur, J. Paserba, V. Ajjarapu, G. Andersson, A. Bose, C. Canizares, N. Hatziargyriou, D. Hill, A. Stankovic, C. Taylor, T. Van Cutsem, and V. Vittal, "Definition and classification of power system stability IEEE/CIGRE joint task force on stability terms and definitions," *IEEE Trans. Power Syst.*, vol. 19, no. 3, pp. 1387–1401, Aug. 2004.

[4] A. Ghosh and D. Chatterjee, "Transient stability assessment of power systems containing series and shunt compensators," *IEEE Trans. Power Syst.*, vol. 22, no. 3, pp. 1210–1220, Aug. 2007.

[5] H. Fujita and H. Akagi, "Voltage-regulation performance of a shunt active filter intended for installation on a power distribution system," *IEEE Trans. Power Electron.*, vol. 22, no. 3, pp. 1046–1053, May 2007.

[6] D. Basic, V. Ramsden, and P. Muttik, "Harmonic filtering of high-power 12-pulse rectifier loads with a selective hybrid filter system," *IEEE Trans. Ind. Electron.*, vol. 48, no. 6, pp. 1118–1127, Dec. 2001.

[7] G. Franklin, J. Powell, and M. Workman, *Digital Control of Dynamic Systems*, 3rd ed. Meno Park, CA, USA: Addison-Wesley/Longman, 1998.

[8] D. Holmes and T. Lipo, *Pulse Width Modulation for Power Converters: Principles and Practice*. Piscataway, NJ, USA: Wiley/IEEE Press, 2003.

[9] P. Krause, O. Wasynczuk, and S. Sudhoff, *Analysis of Electric Machinery and Drive Systems*. Piscataway, NJ, USA: Wiley/IEEE Press, 2002.

[10] C. Chen, *Linear System Theory and Design*, 3rd ed. New York, USA: Oxford Univ. Press, 1999.

[11] H. Kanaan, S. Georges, N. Mendalek, A. Hayek, and K. Al-Haddad, "A linear decoupling control for a PWM three-phase four-wire shunt active power filter," in *Proc. IEEE Mediterranean Electrotechnical Conf.*, 2008, pp. 610–618.

[12] R. Crosier and S. Wang, "A 4800-V grid-connected electric vehicle charging station that provides STACOM-APF functions with a bi-directional, multi-level, cascaded converter," in *Proc. IEEE Appl. Power Electron. Conf. Exposition*, 2012, pp. 1508–1515.

[13] L. da Silva, L. de Lacerda de Oliveira, V. da Silva, G. Torres, E. Bonaldi, and R. Rossi, "Speeding-up dynamic response of active power conditioners," in *Proc. IEEE Canadian Conf. Electr. Comput. Eng.*, 2003, pp. 347–350.

[14] V. Soares, P. Verdelho, and G. Marques, "Active power filter control circuit based on the instantaneous active and reactive current i_d–i_q method," in *Proc. IEEE Power Electron. Specialist Conf.*, 1997, pp. 1096–1101.

[15] L. Haichun, X. Lizhi, and X. Shaojun, "A method for detecting fundamental current based on 2nd order series resonant filter," in *Proc. IEEE Int. Power Electron. Motion Conf.*, 2009, pp. 2411–2415.

[16] S. Wang, R. Crosier, and Y. Chu, "Investigating the power architectures and circuit topologies for megawatt superfast electric vehicle charging stations with enhanced grid support functionality," in *Proc. IEEE Int. Electric Vehicle Conf.*, 2012, pp. 1–8.

[17] Y. Chu and S. Wang, "Bi-directional isolated DC-DC converters with reactive power loss reduction for electric vehicle and grid support applications," in *Proc. IEEE Transp. Electrification Conf.*, 2012, pp. 1–6.

[18] T. Kawabata, T. Miyashita, and Y. Yamamoto, "Deadbeat control of three phase PWM inverter," *IEEE Trans. Power Electron.*, vol. 5, no. 1, pp. 21–28, Jan. 1990.

[19] R. Crosier, S. Wang, and Y. Chu, "Modeling of a grid-connected, multifunctional electric vehicle charging station in active filter mode with DQ theory," in *Proc. IEEE Energy Conversion Congress Exposition*, 2012, pp. 3395–3402.

[20] C. Wan, M. Huang, C. Tse, S. Wong, and X. Ruan, "Irreversible instability in three-phase voltage-source converter connected to non-ideal power grid with interacting load," in *Proc. IEEE Energy Congress Exposition*, Sep. 2012, pp. 1406–1411.

[21] Y. Mohammed, "Mitigation of converter-grid resonance, grid-induced distortion, and parametric instabilities in converter-based distributed generation," *IEEE Trans. Power Electron.*, vol. 26, no. 3, pp. 983–996, Mar. 2011.

[22] T. Lee and S. Hu, "Discrete frequency-tuning active filter to suppress harmonic resonances of closed-loop distribution power systems," *IEEE Trans. Power Electron.*, vol. 26, no. 1, pp. 137–148, Jan. 2011.

Russell Crosier (S'12) received the B.S.E.E and M.S.E.E. degrees from the University of Texas-San Antonio, San Antonio, TX, USA, in 2006 and 2012, respectively.

From 2006 to 2008, he was with the Department of Energy, Montana State University, Bozeman, USA, working on a project in the area of power electronics and power factor correction His research interests include stability of grid-connected power electronics and the control of a multimegawatt, superfast, electric vehicle charging station.

Shuo Wang (S'03–M'06–SM'07) received the Ph.D. degree from Virginia Tech, Blacksburg, UA, USA, in 2005.

He has been with the Department of Electrical and Computer Engineering, University of Texas-San Antonio, San Antonio, USA, since 2010. He has published more than 90 journal and conference papers. He holds six U.S. patents and has one more pending.

Dr. Wang received the Best Transaction Paper Award from the IEEE Power Electronics Society in 2006 and two William M. Portnoy Awards from the IEEE Industry Applications Society in 2004 and 2012, respectively. In March 2012, he received the prestigious National Science Foundation CAREER Award. He is an Associate Editor for the IEEE TRANSACTIONS ON INDUSTRY APPLICATIONS.